arXiv:astro-ph/0004221v1 17 Apr 2000

COLOR GRADIENTS IN EARLY-TYPE GALAXIES IN CLUSTERS AT THE REDSHIFT FROM 0.37 TO 0.56

Naoyuki Tamura and Kouji Ohta

Department of Astronomy, Faculty of Science, Kyoto University, Kyoto 606-8502, Japan

tamura@kusastro.kyoto-u.ac.jp

Received _____; accepted _____

ABSTRACT

Color gradients in elliptical galaxies in distant clusters ($z = 0.37 - 0.56$) are examined by using the archival deep imaging data of Wide Field Planetary Camera 2 (WFPC2) on-board the Hubble Space Telescope (HST). Obtained color gradients are compared with the two model gradients to examine the origin of the color gradients. In one model, a color gradient is assumed to be caused by a metallicity gradient of stellar populations, while in the other one, it is caused by an age gradient. Both of these model color gradients reproduce the average color gradient seen in nearby ellipticals, but predict significantly different gradients at a redshift larger than $\sim$0.3. Comparison between the observed gradients and the model gradients reveals that the metallicity gradient is much more favorable as the primary origin of color gradients in elliptical galaxies in clusters. The same conclusion has been obtained for field ellipticals by using those at the redshift from 0.1 to 1.0 in the Hubble Deep Field-North by Tamura et al. (2000). Thus, it is also suggested that the primary origin of the color gradients in elliptical galaxies does not depend on galaxy environment.

Subject headings: galaxies: elliptical and lenticular, cD— galaxies: evolution— galaxies: formation

1. INTRODUCTION

It has been known that nearby elliptical galaxies have color gradients; colors in an elliptical galaxy gradually become bluer with increasing radius (e.g., Vader et al. 1988; Franx, Illingworth, & Heckman 1989; Peletier et al. 1990a; Peletier, Valentijn, & Jameson 1990b, Goudfrooij et al. 1994; Michard 1999). Since many of elliptical galaxies show radial

gradients in metal absorption line strengths such as Mg_2, Fe_1(5270 Å) and Fe_2(5335 Å) (e.g., Carollo, Danziger, & Buson 1993; Davies, Sadler, & Peletier 1993; Gonzalez 1993; Kobayashi & Arimoto 1999), the origin of the color gradients has been naively interpreted to be the metallicity gradients.

However, such an interpretation for the origin of the color gradient is premature, because both metallicity gradient and age gradient in stellar population can cause the same color gradient, and we cannot distinguish the cause for the gradient. This is called *age-metallicity degeneracy*, which was originally pointed out by Worthey, Trager, & Faber (1996) in terms of the origin of the color-magnitude relation of nearby elliptical galaxies (see also Arimoto 1996). In order to break this degeneracy and to know the primary origin of the color gradients in elliptical galaxies, comparing the observed color gradients in distant ellipticals with predicted model gradients caused by either the metallicity gradient or the age gradient is a very effective approach, as was successful for examining the origin of the color-magnitude (CM) relation (Kodama & Arimoto, 1997). Tamura et al. (2000; hereafter called Paper I) constructed the two models both of which reproduce a typical color gradient of elliptical galaxies at $z = 0$ using a population synthesis model. In one model, the mean metallicity of the stellar population decreases with increasing radius at a fixed old mean age. While in the other one, the mean age decreases with a radius at a fixed mean metallicity. These models were then made evolve back in time. The evolution of color gradients thus predicted are confronted with the observed ones in distant ($z = 0.1 \sim 1.0$) ellipticals sampled from the *Hubble Deep Field-North* (HDF-N; Williams et al. 1996). As a result, Paper I found that the metallicity gradient is the primary origin of color gradients and the age gradient model cannot reproduce the observed gradient at such redshift.

The elliptical galaxies in the HDF-N, however, are only those in field environment. It has never been obvious that ellipticals in clusters evolve similarly as those in field. In

rich clusters, it has been found that the color-magnitude relation still holds even at around $z \sim 1$ (e.g., Stanford, Eisenhardt, & Dickinson 1998) and these observational results seem to favor the classical monolithic collapse scenario associated with the galactic wind and high-z formation (e.g., $z > 3$) of elliptical galaxies (e.g., Kodama et al. 1998). However, this kind of evolution has not been established for ellipticals in lower density environment (but see Kodama, Bower, & Bell 1998). Some predictions either theoretically or observationally show that field ellipticals formed by recent (at $z \leq 1$) merging processes (e.g., Baugh, Cole, & Frenk 1996; Barger et al. 1999). An internal structure of a galaxy such as a metallicity gradient and an age gradient must depend on its formation process. If cluster ellipticals pass different formation histories from those for field ellipticals, their internal structures, thus the origin of the color gradients, may not be the same. Or some environmental effects on color gradients may exist. Thus, the same approach is needed for cluster ellipticals to clarify the origin of their color gradients.

It is noted that dust extinction in elliptical galaxies may also have some effects on the color gradients (Goudfrooij & de Jong 1995; Wise & Silva 1996; Silva & Wise 1996). However, about half of the detection towards ellipticals in far infrared with IRAS are around 3σ threshold and confirmation is needed to be definitive (Bregman et al. 1998). In addition, spatial distribution of dust in an elliptical galaxy as well as dust mass which could affect a color gradient are not established yet. These are still open problems and will be examined in detail in our forthcoming papers. Therefore, in this paper, we have chosen to focus on age and metallicity effects only.

This paper is organized as follows. The sample selection and data analysis of elliptical galaxies are described in § 2. Histograms of color gradients are presented in § 3 together with the representative color profiles of the sample ellipticals. Discussion is given in § 4. The cosmological parameters adopted throughout this paper are the same as those in Paper

I; $H_0 = 50$ km s^{-1} Mpc^{-1}, $\Omega_0 = 0.2$ and $\Lambda = 0$.

2. DATA AND SAMPLE SELECTION

In order to examine color gradients in elliptical galaxies in distant clusters, deep imaging data with a high angular resolution are necessary in more than two bands. Thus, we choose to use the archival data taken with the WFPC2 on-board the HST. Smail et al. (1997) obtained deep imaging data of 11 distant rich clusters at the redshift from 0.37 to 0.56, most of which have exposure times more than 10,000 sec to examine their morphology in detail, and presented catalogs of the detected objects. In this paper, their reduced imaging data which are available at their web site[1] are used. From these data, we select six clusters whose images were taken in two bands to obtain galaxy colors. Cluster IDs and their basic properties taken from Smail et al. (1997) are given in Table 1. Among these clusters, Cl 0024+16, Cl 0016+16, and Cl 0054−27 are classified as high concentration clusters and Cl 0939+47 and Cl 0412−65 are low concentration clusters (Dressler et al. 1997). For A370 and Cl 0939+47, the images of their outer fields were taken. Therefore, environmental effects on color gradients may be examined.

Early type galaxies (E, E/S0, S0/E) in these clusters are sampled based on the catalog by Smail et al. (1997). Since our main interest is to examine their color gradients, high signal-to-noise ratio (S/N) is required and thus galaxies brighter than the apparent magnitude of 21 mag in I_{814} band are selected in all of the sample clusters. This apparent magnitude roughly corresponds to the absolute magnitude of -20 mag in V band. Our sample galaxies are listed in Table 2 with their basic parameters, most of which are taken from Smail et al. (1997). In each cluster, the sample galaxies form the tight CM relations

[1]http://star-www.dur.ac.uk/~irs/morphs.html

as shown in Figure 1, though the relations in A370, Cl 0939+47, and Cl 0412−65 are somewhat loose. Since Cl 0939+47 and Cl 0412−65 are classified as low concentration clusters, and the outer regions of the clusters were imaged for A370 and Cl 0939+47, some environmental effects on the CM relations might be seen. However, a discussion for this subject is beyond our scope in this paper. In the figure, a solid square with an open circle shows the object removed from the following analysis, because their color gradients could not be derived accurately enough to use our discussion due to their low signal-to-noise ratios (S/Ns) or due to their close positions to an edge of the image.

3. PROFILES AND COLOR GRADIENTS

In deriving color profiles of the sample galaxies, we should take care of a positional coincidence between a blue image and a red image, and a difference of the sizes of point spread functions (PSFs) between the two images. (One pixel corresponds to $0\farcs10$ for the Wide Field Cameras and $0\farcs046$ for the Planetary Camera.) Positional displacement between a blue image and a red one causes spurious asymmetry of a color distribution in a galaxy and has a serious effect on the color gradient. We examined the centroids of the sample galaxies in both blue and red images and corrected a displacement, if a systematic shift between the two images in each cluster was found. The sizes of PSFs should be also estimated and be adjusted between blue and red images. We simulated the PSF at each position of a sample galaxy in each band by using TinyTim v4.4 (Krist 1995; Krist & Hook 1997), and corrected the difference of the sizes between the two images, which were estimated by fitting a Gaussian to the PSFs. Sky value was determined by "mode" in an annulus with an inner radius of $9''$ and a width of $3''$ by using the "phot" task in the IRAF apphot package and the obtained sky was subtracted.

We next made azimuthally averaged radial surface brightness profiles in both blue and

red images with a radial sampling of 0.″1. These profiles in each galaxy are made along the ellipses fitted with a fixed position angle to the isophotes of the galaxy images in the red band. (The position angles are taken from Table 2A by Smail et al. (1997).) Thus the surface brightness profiles in the two bands are derived based on the same fitted elliptical isophotes. In Figure 2, representative surface brightness profiles of our sample galaxies are shown. The profiles of the brightest, intermediate, and the faintest sample galaxies in each cluster are shown in top, middle, and bottom panels, respectively. The profiles of almost all the galaxies in our sample are well represented by the $r^{1/4}$ law. To derive color profiles, the surface brightness profile in the red band is subtracted from the profile in the blue band. Figure 3 shows the resulting color profiles with the same arrangement as in Figure 2. An error bar to each data point includes a photometric error, a local sky subtraction error (1% of a sky value around each object is adopted), and a dispersion of colors along each elliptical isophote. It is important to describe here the two dimensional color distribution in the sample galaxies. The color maps were constructed by dividing the blue image by the red image after adjusting the positional displacement and difference of the sizes of the PSFs. Almost all the color maps show smooth color distribution and do not show any asymmetric or peculiar features. Thus the color profiles well represent the color distribution in each galaxy.

Finally, slopes of the color profiles, i.e., color gradients, in the sample galaxies are derived by the least square fitting within effective radii, which are obtained from the surface brightness profiles in the red band assuming the $r^{1/4}$ law. The fitting for the color gradients are done after removing data points with errors larger than 0.3 mag. We do not derive the gradients of the profiles with accepted data points fewer than 3. The average number of the data points used for the fitting is about 8 and the rejected objects are minor. Resulting color gradients in the sample galaxies are listed in Table 2 with the 1σ fitting errors. Figure 3 indicates resulting slopes of the color gradients as well as the slopes with $\pm 1\sigma$. In this

figure, abscissa refers to logarithm of a radius normalized by the outermost radius (r_f) used for the fitting in each color profile. For most of the sample galaxies, r_f is roughly equal to r_e.

Figure 4 shows a histogram for the color gradients of the sample galaxies in each cluster. Each bin of the histograms is set to be 0.2 mag/dex which is comparable to the average value of the fitting error. It is found that the distributions of the gradients are very narrow except for a few outliers, which are #535 and #738 in Cl 0024+16, #2005 in Cl 0939+47, and #2050 in Cl 0016+16. The former three are significantly out of the CM relation towards the blue side, but the last one is almost on the relation. Considering that the range of the distribution of the color gradients is comparable with or only slightly larger than the estimated error for the slopes, the intrinsic dispersions of the color gradients must be considerably small. (The dispersion of the color gradients in nearby elliptical galaxies is about 0.04 mag/dex (Peletier et al. 1990a; Paper I).) It is intriguing that the color gradients of elliptical galaxies are uniform even at intermediate redshift. Furthermore, this encourages the comparison between model gradients and observed gradients in distant clusters, despite rather large errors for the observed slopes.

4. ORIGIN OF COLOR GRADIENTS IN CLUSTER ELLIPTICALS

4.1. Models

In order to examine whether the origin of the color gradient is the stellar metallicity or the age, we adopt the same approach as that in Paper I and the reader should refer to it in detail. We briefly summarize it here.

An observed color gradient can be reproduced by either a metallicity gradient or an age gradient of stellar populations in an elliptical galaxy at $z = 0$. However, since the color

gradient caused by a metallicity gradient is expected to follow a different evolution from that by an age gradient, the origin of the color gradients can be found by comparing the observed ones at high redshift with those predicted by model. For this purpose, using the population synthesis model (Kodama & Arimoto 1997; Kobayashi, Tsujimoto, & Nomoto 2000), we construct the two model galaxies; one model galaxy has the color gradient made by the pure metallicity gradient (thereafter called *metallicity gradient model*) without age gradient, and the other made by the pure age gradient (*age gradient model*) without metallicity gradient. In the metallicity gradient model, the metallicity gradient is produced by assuming that a galactic wind blowed later in the inner region in an elliptical galaxy; star formation continued longer and thus the mean stellar metallicity became higher at the inner region. For the age gradient model, star formation started earlier in the inner region and thus the mean age of stellar populations is older than that in the outer region. The stellar population in each region in an elliptical galaxy is assumed to be made by a single burst and to evolve independently of other regions. Model parameters used here are set to the same as those in Paper I, which are chosen so as to reproduce the typical color gradient at $z = 0$. The mean value of $\Delta(B-R)/\Delta \log r$ of -0.09 mag/dex obtained by Peletier et al. (1990a) is adopted as the typical color gradient at $z = 0$. Note that these model galaxies must be old ($8 \sim 15$ Gyr) to reproduce colors in nearby elliptical galaxies. Then, we calculate the spectral evolution in each region of the model galaxies and their color gradients at any redshifts using the response functions including each filter on the HST. It should be emphasized that we do not intend to study physical formation process of elliptical galaxies in this paper, but aim at depicting the evolution of the color gradient caused by either metallicity gradient or age gradient to be compared with the observed ones. Actual physical process that made the metallicity/age gradient may be different from our brief ideas presented in the model description. However it is not a problem here, because once such gradient formed, subsequent evolution of the stellar population is unique and does not

depend on the formation process.

The two lines in each panel of Figure 5 show the evolutionary track of the model color gradients; the solid curve indicates the evolution for the metallicity gradient model and the dotted curve for the age gradient model. The model color gradient by the metallicity gradient is almost constant with a redshift within $z \sim 1$, while that by the age gradient changes abruptly and shows a quite steep gradient even at $z = 0.3$. We will compare the model gradients with the observed ones in the next subsection.

4.2. Model vs observation

The mean values of the color gradients in each cluster sample are plotted at their redshifts in Figure 5. An error bar attached to each point indicates a mean error of the gradients in each cluster. As clearly shown, the metallicity gradient is much more favorable as the origin of the color gradients. This result does not depend on cosmological parameters or parameters for an evolutionary model of galaxy within a reasonable range, and does not change even if we consider the dispersion of the color gradients in the sample galaxies (see Figure 4) and that in nearby ellipticals (~ 0.04 mag/dex). Although the sample galaxies of which memberships in the clusters are spectroscopically confirmed are minor (Dressler et al. 1999), background or foreground contaminations are not expected to affect the result for the origin of the color gradients, because the result does not change even if we remove the galaxies which significantly deviate from the CM relation in each cluster. The color gradients in several sample galaxies may be affected by other galaxies close to them, and the color profile of a galaxy which locates close to an edge of the chip or on a joint between the cameras may be somewhat spurious. However, our result still holds even after removing the galaxies which may suffer from these effects.

Considering the result in Paper I, in both cluster and field, the primary origin of the color gradients in elliptical galaxies is considered to be the stellar metallicity. However, it is interesting to point out that the mean values of the color gradients seem to deviate upwards from the line for the metallicity gradient model. Our models are calibrated by the color gradients seen in nearby ellipticals by Peletier et al. (1990a), in which most of the sample ellipticals reside in field or group environment. Therefore, the upward deviation might indicate an environmental effect on the color gradients of elliptical galaxies between in rich clusters and in field. However, the correlation between the mean value and the degree of the concentration in each cluster is not seen. In addition, the mean gradients of the clusters of which outer field images were taken do not show larger values than others. Further detailed study on the color gradients in cluster ellipticals and field ones at $z = 0$ as well as at high redshift should be done in the future.

We would like to thank C. Kobayashi, N. Arimoto, and T. Kodama for fruitful collaboration in Paper I. This work was financially supported in part by Grant-in-Aid for the Scientific Research (No. 11740123) by the Ministry of Education, Science, Sports and Culture of Japan.

REFERENCES

Arimoto, N. 1996, in From Stars to Galaxies, eds. C. Leitherer, U. Fritze-v. Alvensleben, & J. Huchra, ASP Conf. Ser. Vol. 98, p. 287

Barger, A., Cowie, L. L., Trentham, N., Fulton, E., Hu, E. M., Songaila, A., & Hall, D. 1999, AJ, 117, 102

Baugh, C. M., Cole, S., & Frenk, C. S. 1996, MNRAS, 283, 1361

Bregman, J. N., Snider, B. A., Grego, R., & Cox, C. V. 1998, ApJ, 499, 670

Carollo, C. M., Danziger, I. J., & Buson, L. 1993, MNRAS, 265, 553

Davies, R. L., Sadler, E. M., & Peletier, R. F. 1993, MNRAS, 262, 650

Dressler, A., Oemler, A. Jr., Couch, W. J., Smail, I., Ellis, R. S., Barger, A., Butcher, H., Poggianti, B. M., & Sharples, R. 1997, ApJ, 490, 577

Dressler, A., Smail, I., Poggianti, B. M., Butcher H., Couch, W. J., Ellis, R. S., & Oemler, A. Jr. 1999, ApJS, 122, 51

Franx, M., Illingworth, G., & Heckman, T. 1989, AJ, 98, 538

Gonzalez, J. J. 1993, PhD thesis, Univ. of California

Goudfrooij, P., Hansen, L., Jørgensen, H. E., Nørgaard-Nielsen, H. U., de Jong, T., & van den Hoek, L. B. 1994, A&AS, 104, 179

Goudfrooij, P., & de Jong, T. 1995, A&A, 298, 784

Kobayashi, C., & Arimoto, N. 1999, ApJ, 527, 573

Kobayashi, C., Tsujimoto, T., & Nomoto, K. 2000, ApJ, in press

Kodama, T., & Arimoto, N. 1997, A&A, 320, 41

Kodama, T., Arimoto, N., Barger, A. J., & Aragón-Salamanca, A. 1998, A&A, 334, 99

Kodama, T., Bower, R. G., & Bell, E. F. 1998, MNRAS, 306, 561

Krist, J. E. 1995, in Astronomical Data Analysis Software and Systems IV, eds. Shaw, R. A., Payne, H. E., & Hayes, J. M. E., ASP conf. Ser. Vol. 77, p. 349

Krist, J. E., & Hook, R. 1997, The Tiny Tim (Version 4.4) User's Guide

Michard, R. 1999, A&AS, 137, 245

Peletier, R. F., Davies, R. L., Illingworth, G. D., Davis, L. E., & Cawson ,M. 1990a, AJ, 100, 1091

Peletier, R. F., Valentijn, E. A., & Jameson, R. F. 1990b, A&A, 233, 62

Silva, D. R., & Wise, M. W. 1996, ApJ, 457, L15

Smail, I., Dressler, A., Couch, W. J., Ellis, R. S., Oemler, A. Jr., Butcher, H., & Sharples, R. 1997, ApJS, 110, 213

Stanford, S. A., Eisenhardt, P. R., & Dickinson, M. 1998, ApJ, 492, 461

Tamura, N., Kobayashi, C., Arimoto, N., Kodama, T., & Ohta, K. 2000, AJ, in press (Paper I)

Vader, J. P., Vigroux, L., Lachièze-Rey, M., & Souviron, J. 1988, A&A , 203, 217

Williams, R. E., et al. 1996, AJ, 112, 1335

Wise, M. W., & Silva, D. R. 1996, ApJ, 461, 155

Worthey, G., Trager, S. C., & Faber, S. M. 1996, in Fresh Views of Elliptical Galaxies, eds. A. Buzzoni, A. Renzini, & A. Serrano, ASP Conf. Ser. Vol. 86, p. 203

This manuscript was prepared with the AAS LaTeX macros v5.0.

Table 1: Sample Clusters

ID	z	Image Center		Exposure (sec)	Exposure(sec)
		α(J2000)	δ(J2000)	(F555W)[a]	(F814W)
A370 Field 2	0.37	02h40m01.1s	$-01°36'45''$	8000	12600
Cl 0024+16	0.39	00h26m35.6s	$+17°09'43''$	23400	13200
Cl 0939+47 Field 2	0.41	09h43m02.5s	$+46°56'07''$	4000	6300
Cl 0412−65	0.51	04h12m51.7s	$-65°50'17''$	12600	14700
Cl 0016+16	0.55	00h18m33.6s	$+16°25'46''$	12600	16800
Cl 0054−27	0.56	00h56m54.6s	$-27°40'31''$	12600	16800

[a]For Cl 0024+16, the exposure time in the F450W band image.

Table 2: Sample galaxies

- A370

ID	I_{814} (mag)	$V_{555}-I_{814}$ (mag)	$\Delta(V_{555}-I_{814})/\Delta\log r$ (mag/dex)	N[a]
192	18.712	1.897	0.11±0.06	16
221	20.828	2.345	0.11±0.39	4
230	18.847	1.578	−0.02±0.12	7
231	19.641	1.926	0.11±0.14	6
232	18.911	2.067	−0.08±0.12	8
265	20.491	1.786	−0.09±0.20	6
289	20.539	1.575	0.17±0.16	5
351	20.562	1.602	−0.08±0.11	9
377	18.977	2.021	−0.04±0.08	17
458	20.299	1.817	0.11±0.29	6
469	20.346	0.915	–	–
487	19.071	1.867	0.00±0.08	16
2024	20.955	2.343	−0.21±0.40	4

[a]Number of the data points in a color profile for deriving a color gradient.

Table 2: —Continue

- Cl 0024+16

ID	I_{814} (mag)	$B_{450} - I_{814}$ (mag)	$\Delta(B_{450} - I_{814})/\Delta \log r$ (mag/dex)	N
89	19.947	3.199	–	–
112	19.519	3.278	−0.00±0.11	13
113	18.892	3.404	−0.13±0.09	14
137	20.827	3.391	−0.52±0.45	4
145	20.717	3.251	0.18±0.38	4
147	19.411	3.290	−0.27±0.12	10
169	20.795	3.255	–	–
179	19.654	3.559	−0.01±0.18	7
261	19.623	3.310	0.06±0.23	7
268	19.400	3.296	0.14±0.19	8
280	18.200	3.481	−0.22±0.06	30
294	19.959	3.296	0.42±0.21	6
304	18.469	3.419	−0.28±0.06	26
327	20.759	3.173	–	–
334	19.567	3.389	−0.03±0.15	8
337	20.069	3.348	0.16±0.37	4
342	18.680	3.412	−0.05±0.08	20
343	18.348	3.506	−0.28±0.05	30
353	20.557	3.220	0.01±0.40	4
362	18.901	3.367	−0.04±0.12	8
365	18.309	3.403	−0.17±0.06	27

Table 2: — Continue

- Cl 0024+16 — Continue

ID	I_{814} (mag)	$B_{450} - I_{814}$ (mag)	$\Delta(B_{450} - I_{814})/\Delta \log r$ (mag/dex)	N
403	19.349	3.317	−0.55±0.14	11
419	19.573	3.444	−0.13±0.19	7
479	20.768	3.170	0.14±0.39	4
514	19.883	3.325	−0.34±0.19	7
521	20.259	3.318	0.22±0.29	5
535	20.343	2.501	−1.68±0.12	17
573	18.353	3.424	−0.19±0.20	10
590	20.201	3.385	–	–
621	18.660	3.405	−0.20±0.07	16
653	19.090	3.311	−0.44±0.12	10
669	20.130	3.282	−0.38±0.24	6
675	20.709	3.216	−0.07±0.37	4
678	20.298	3.256	−0.15±0.30	5
685	20.683	3.196	−0.30±0.38	4
738	20.522	3.208	−3.23±0.35	10
796	19.109	3.450	−0.22±0.11	13
876	19.669	3.315	−0.15±0.23	5
934	20.382	2.259	–	–
3006	20.944	3.118	0.13±0.14	18
3012	20.475	3.367	−0.12±0.15	12

Table 2: —Continue

- Cl 0939+47

ID	I_{814} (mag)	$B_{450} - I_{814}$ (mag)	$\Delta(B_{450} - I_{814})/\Delta \log r$ (mag/dex)	N
31	20.452	2.040	–	–
53	20.247	2.770	−0.17±0.31	5
86	18.769	1.822	0.01±0.04	11
270	19.993	1.866	−0.18±0.12	10
337	20.507	2.209	0.02±0.20	6
404	19.670	2.344	−0.01±0.19	7
426	20.014	1.947	−0.10±0.15	7
429	20.372	2.211	0.18±0.31	5
512	20.972	1.817	0.04±0.24	6
515	20.208	1.997	−0.04±0.13	9
566	20.557	2.010	–	–
2005	20.968	0.700	−0.76±0.31	11

Table 2: —Continue

- Cl 0412−65

ID	I_{814} (mag)	$B_{450} - I_{814}$ (mag)	$\Delta(B_{450} - I_{814})/\Delta \log r$ (mag/dex)	N
431	20.835	2.715	0.03±0.22	7
432	18.992	2.044	−0.08±0.07	18
471	20.074	2.254	0.29±0.16	4
472	19.571	2.330	0.11±0.10	9
635	19.612	2.300	0.06±0.10	14
657	19.597	2.265	0.06±0.10	7
682	20.960	2.183	0.11±0.16	7
695	20.440	2.213	−0.04±0.16	4
772	20.489	0.839	0.23±0.06	14

Table 2: —Continue

- Cl 0016+16

ID	I_{814} (mag)	$B_{450} - I_{814}$ (mag)	$\Delta(B_{450} - I_{814})/\Delta \log r$ (mag/dex)	N
271	20.913	2.387	0.29±0.23	4
438	19.754	2.460	−0.32±0.07	19
461	20.296	2.461	0.19±0.23	4
531	20.692	2.443	–	–
602	20.926	2.469	–	–
606	20.769	2.305	–	–
611	20.232	2.466	0.19±0.16	8
612	19.648	2.574	−0.12±0.10	10
650	19.464	2.482	−0.05±0.07	17
653	19.837	2.384	−0.00±0.13	8
659	19.950	2.441	0.04±0.13	10
724	19.075	2.582	−0.09±0.06	20
725	19.117	2.531	−0.02±0.05	28
726	20.826	2.317	–	–
732	20.009	2.398	0.26±0.18	7
745	20.342	2.519	0.12±0.14	9
802	20.898	2.411	0.06±0.18	7
822	20.956	2.320	0.07±0.17	9
823	20.346	2.387	−0.06±0.12	10
843	20.270	2.372	0.08±0.12	7
903	20.927	2.300	0.14±0.27	4
2026	20.643	2.187	−0.32±0.19	5
2050	20.894	2.366	−1.92±0.42	4
3002	18.894	2.122	–	–

Table 2: —Continue

- Cl 0054−27

ID	I_{814} (mag)	$B_{450} - I_{814}$ (mag)	$\Delta(B_{450} - I_{814})/\Delta \log r$ (mag/dex)	N
165	20.802	2.329	0.25±0.27	5
191	20.225	2.459	−0.11±0.15	9
216	19.627	2.600	−0.01±0.12	9
229	20.393	2.565	0.07±0.20	5
356	20.080	2.469	−0.12±0.17	6
365	20.407	2.345	0.06±0.17	7
440	19.316	2.514	−0.12±0.11	13
529	20.021	2.415	−0.26±0.12	10
711	18.037	1.403	−0.14±0.06	20

Figure Caption

Figure. 1 — Color-magnitude (CM) diagrams for the sample galaxies in the clusters. A solid square with an open circle indicates the object whose color gradient cannot be obtained due to low S/N or the close position to an edge of the image. "#2" in the cluster ID refers to the outer field of the cluster.

Figure. 2 — Azimuthally averaged radial surface brightness profiles of representative galaxies in the sample are presented. The profiles of the brightest, intermediate, and the faintest sample galaxies in each cluster are shown in top, middle, and bottom panels, respectively. Solid squares are the profile in a blue band and open circles in a red band. An object ID is shown at the upper left in each panel.

Figure. 3 — Color profiles and fitted slopes of the representative galaxies in the sample are indicated. The galaxies presented and the arrangement of the panels are the same as those in Figure 2. Among the three solid lines in each panel, the middle one shows the best fit slope. Other two lines show the slopes with $\pm 1\sigma$ of the best fit. Abscissa refers to logarithm of a radius normalized by the outermost radius (r_f) used for the fitting in each color profile.

Figure. 4 — Histograms of the color gradients in the sample galaxies in each sample cluster. A total number of the objects in each histogram is shown at the upper left in each panel and a number in parentheses indicates a total number of the sample galaxies in each cluster. Cluster ID and its redshift are shown on the top of each panel.

Figure. 5 — A mean color gradient in each cluster versus redshift is shown. A solid curve in each panel represents the evolutionary track of the color gradient caused by the metallicity gradient and a dotted curve shows the track by the age gradient (see text in detail).

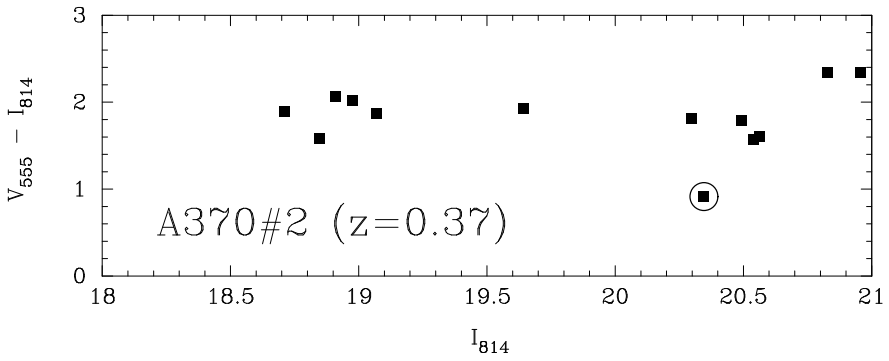
A370#2 (z=0.37)
V555 − I814
I814

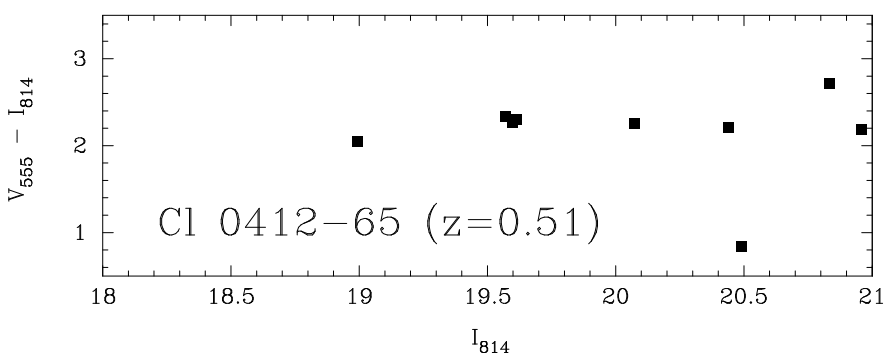
Cl 0412−65 (z=0.51)
V555 − I814
I814

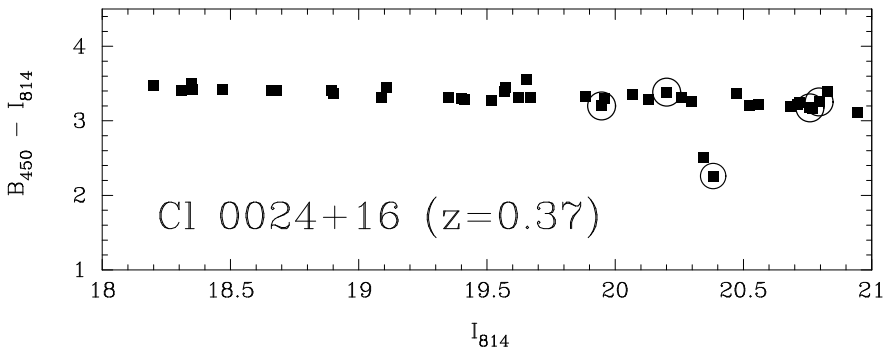
Cl 0024+16 (z=0.37)
B450 − I814
I814

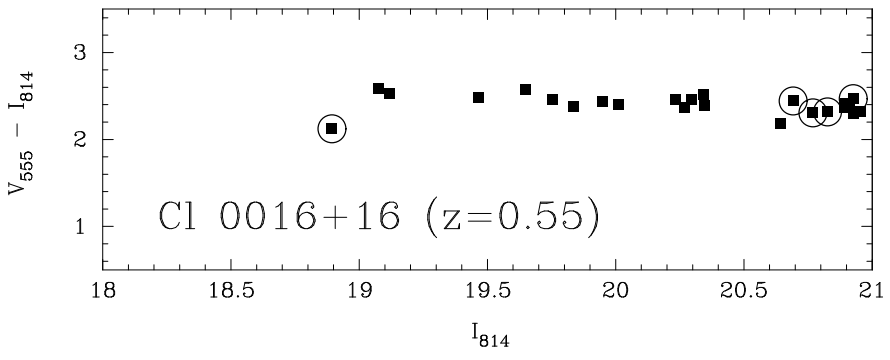
Cl 0016+16 (z=0.55)
V555 − I814
I814

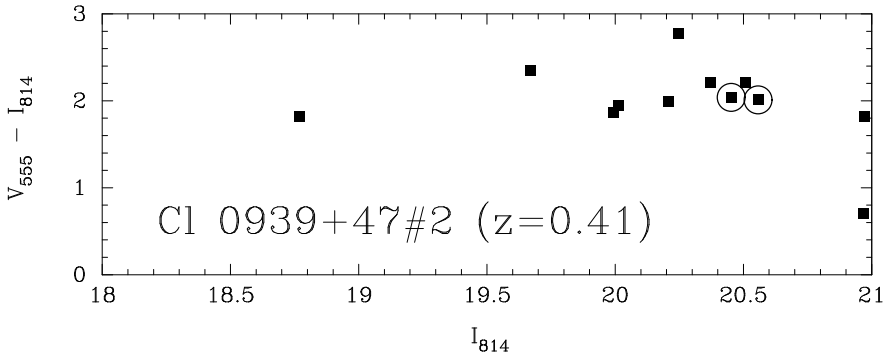
Cl 0939+47#2 (z=0.41)
V555 − I814
I814

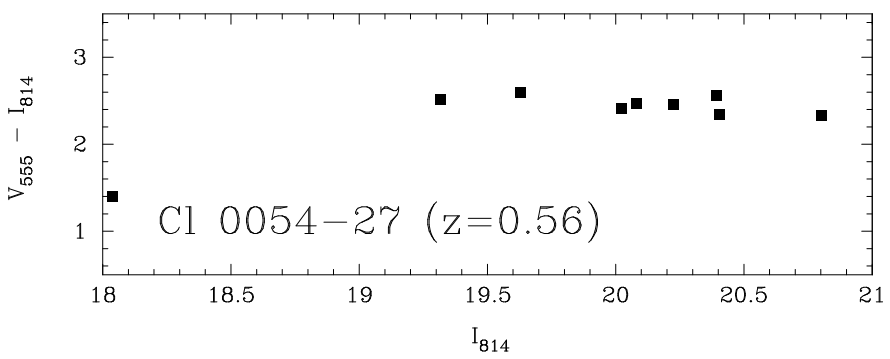
Cl 0054−27 (z=0.56)
V555 − I814
I814

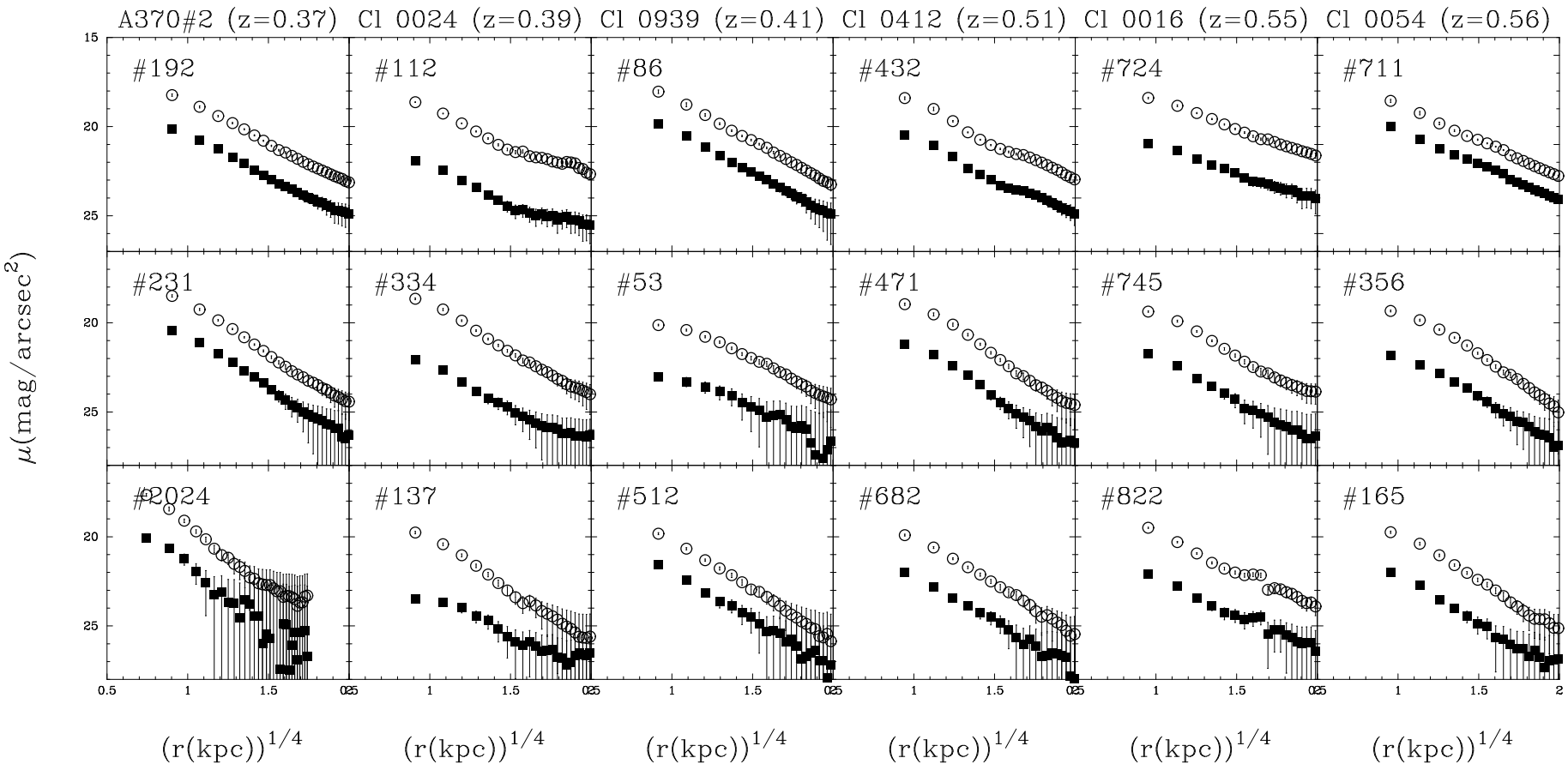
A370#2 (z=0.37)
Cl 0024 (z=0.39)
Cl 0939 (z=0.41)
Cl 0412 (z=0.51)
Cl 0016 (z=0.55)
Cl 0054 (z=0.56)
#192
#112
#86
#432
#724
#711
#231
#334
#53
#471
#745
#356
#2024
#137
#512
#682
#822
#165
μ(mag/arcsec^2)
(r(kpc))$^{1/4}$

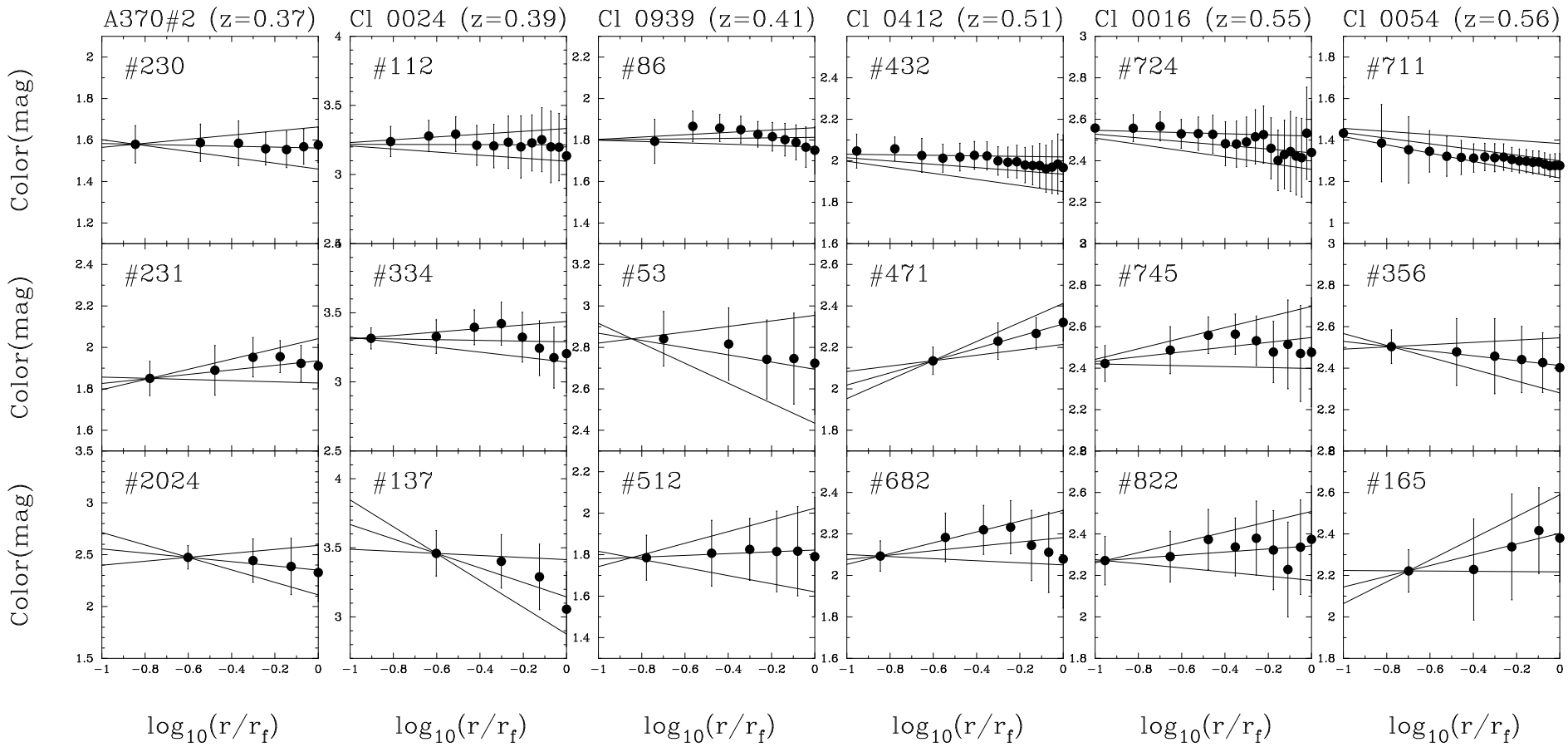
A370#2 (z=0.37)
Cl 0024 (z=0.39)
Cl 0939 (z=0.41)
Cl 0412 (z=0.51)
Cl 0016 (z=0.55)
Cl 0054 (z=0.56)
#230
#112
#86
#432
#724
#711
#231
#334
#53
#471
#745
#356
#2024
#137
#512
#682
#822
#165
Color(mag)
Color(mag)
Color(mag)
log10(r/rf)
log10(r/rf)
log10(r/rf)
log10(r/rf)
log10(r/rf)
log10(r/rf)

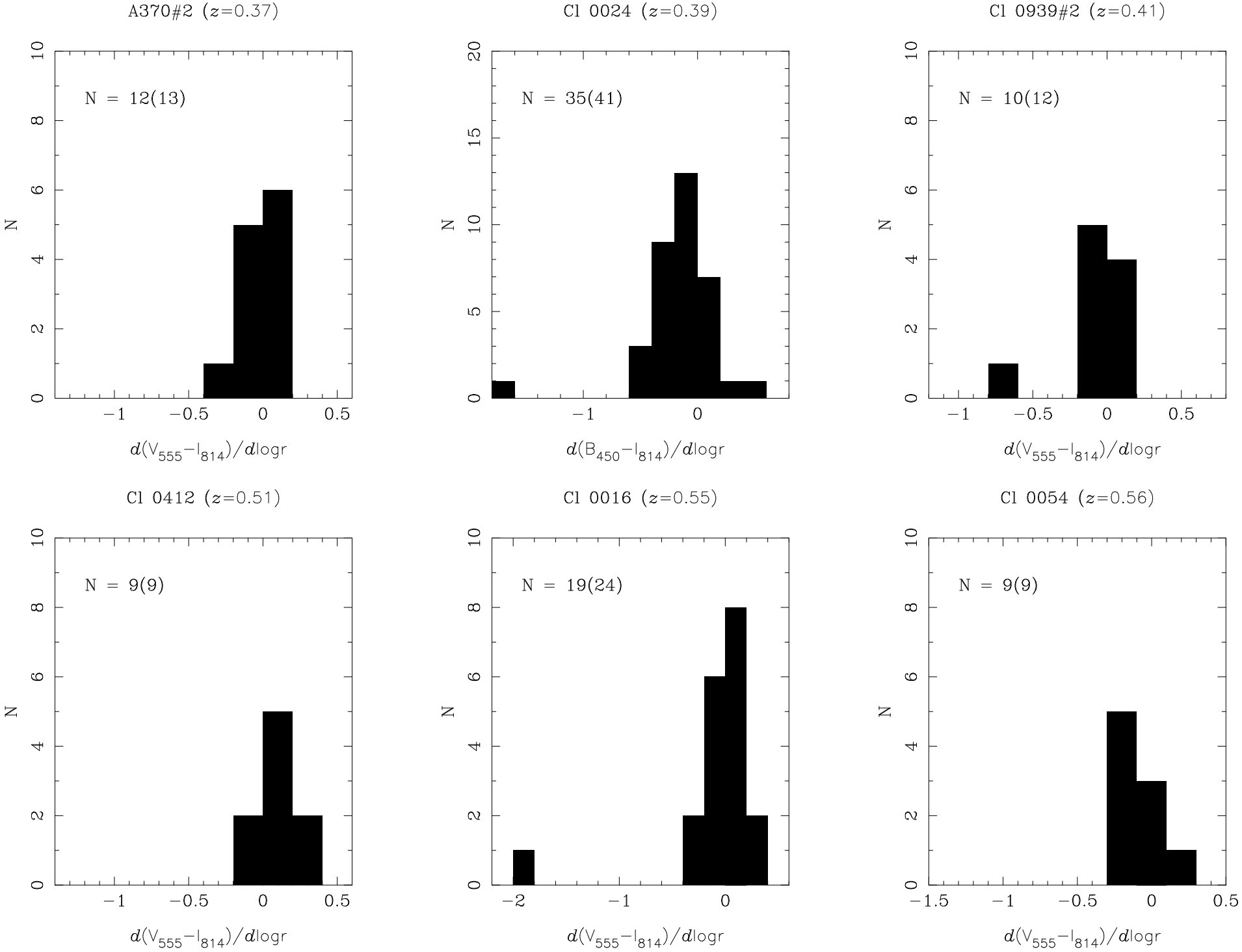
A370#2 (z=0.37)
N = 12(13)
Cl 0024 (z=0.39)
N = 35(41)
Cl 0939#2 (z=0.41)
N = 10(12)
Cl 0412 (z=0.51)
N = 9(9)
Cl 0016 (z=0.55)
N = 19(24)
Cl 0054 (z=0.56)
N = 9(9)
N
d(V555−I814)/dlogr
d(B450−I814)/dlogr

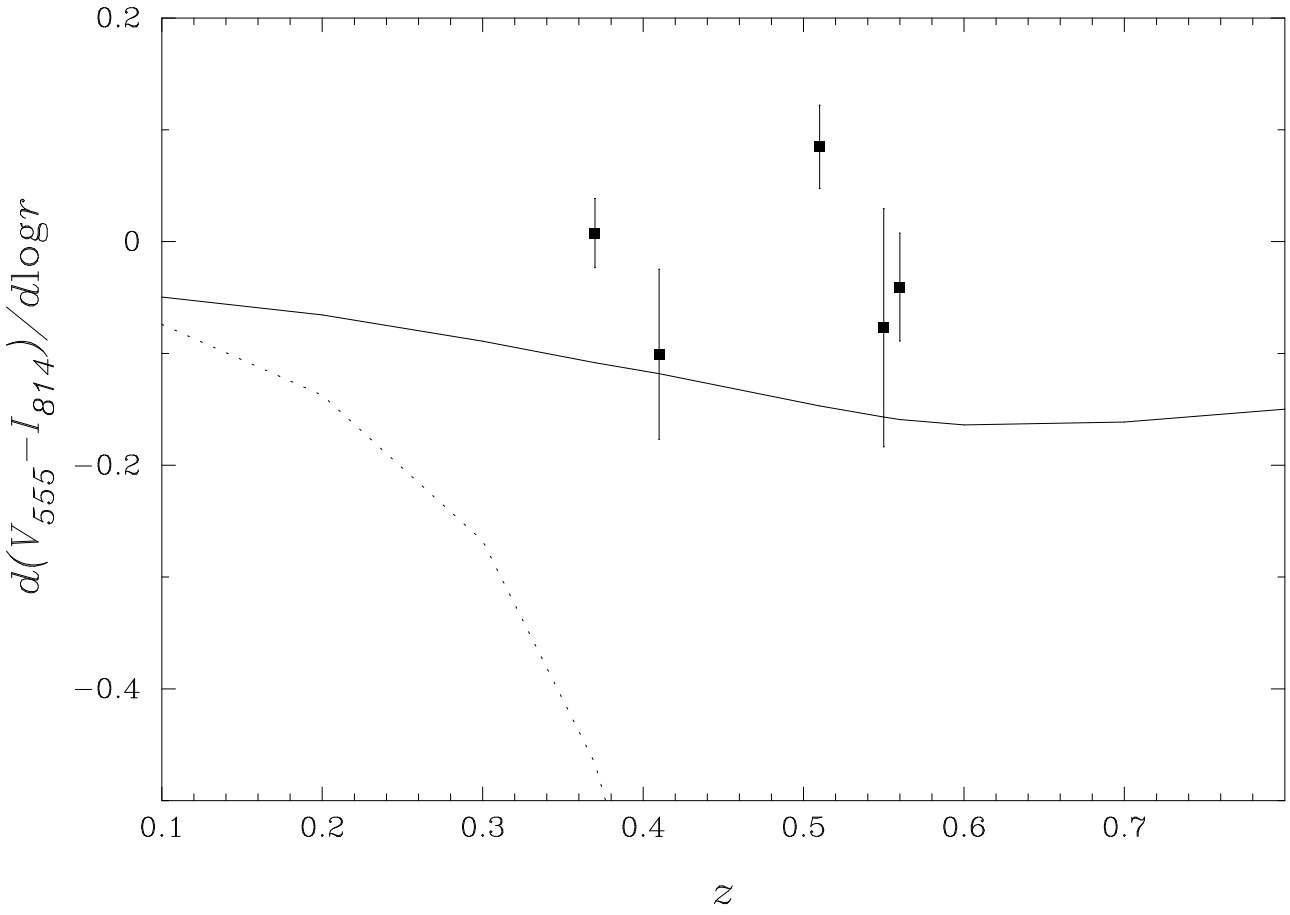
0.2
0
−0.2
−0.4
0.1
0.2
0.3
0.4
0.5
0.6
0.7
$d(V_{555}-I_{814})/d\log r$
z

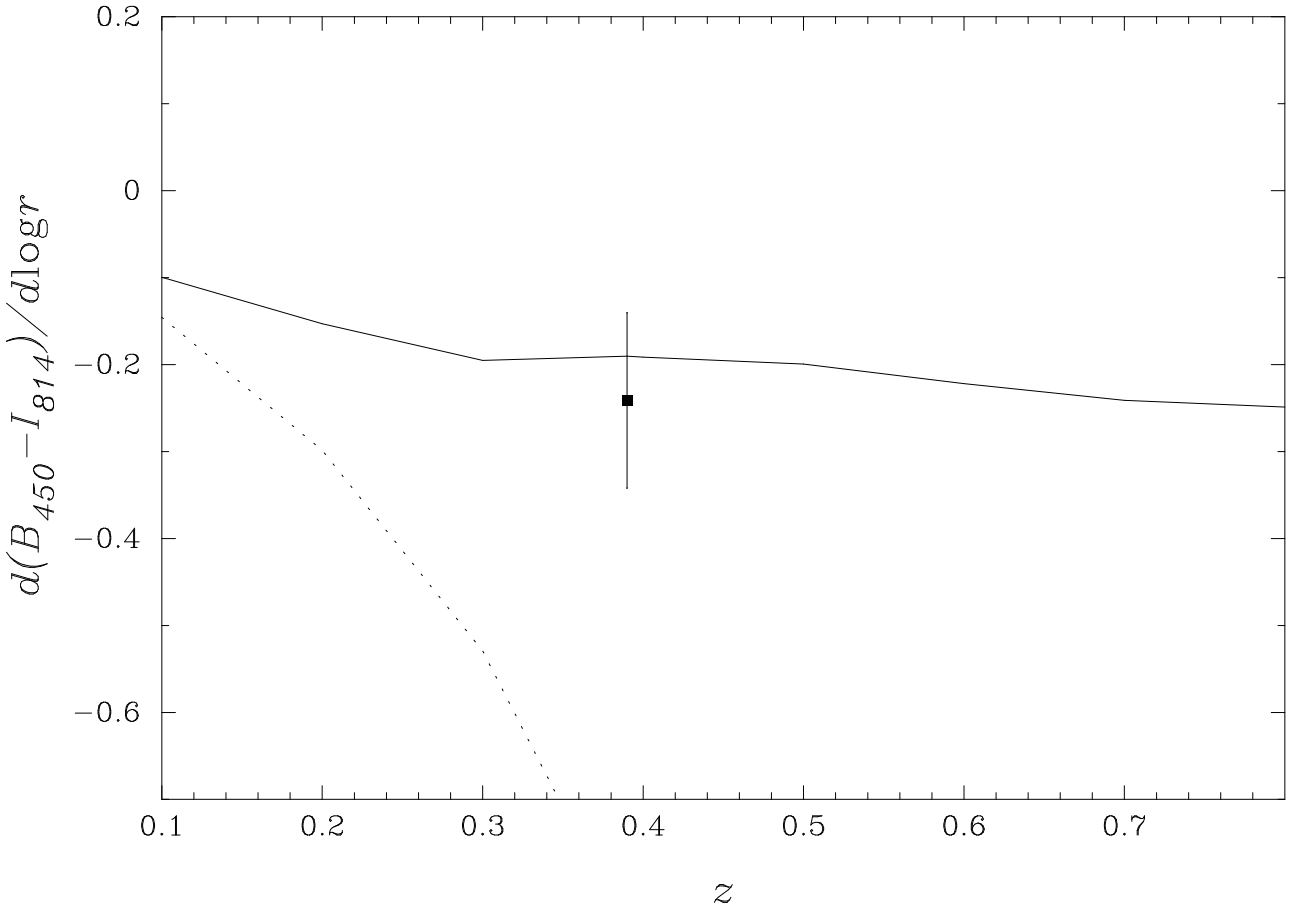
0.2
0
−0.2
−0.4
−0.6
0.1
0.2
0.3
0.4
0.5
0.6
0.7
$d(B_{450}-I_{814})/d\log r$
z